Progress In Electromagnetics Research, PIER 86, 169–198, 2008

A NOVEL ULTRA-COMPACT BROADBAND ANTENNA FOR MICROWAVE BREAST TUMOR DETECTION

H. Kanj and M. Popović

Department of Electrical & Computer Engineering
McGill University
3480 University St., Montréal, Québec H3A 2A7, Canada

Abstract—This paper presents a novel resistively loaded antenna design for microwave breast cancer detection. The antenna is planar and ultra-compact, and can be easily manufactured using PCB technology with embedded thin-film resistive layers. Through numerical simulations, the antenna demonstrates a return loss below −10 dB over a wide frequency range from 2 to 35 GHz. For pulse radiation in the ultra-wideband (UWB) range in a biological medium, the antenna shows an excellent fidelity above 0.95 and a relatively high radiation efficiency of 39.21% in comparison to resistively loaded antennas. In addition, a design rule guideline is presented for designing the antenna to radiate in a specific background medium and with a given lower operating frequency. Finally, a complete microstrip feed design is presented for the antenna operating in the UWB range.

1. INTRODUCTION

Confocal microwave imaging techniques (CMI) are currently being studied as an effective low-cost screening tool for breast cancer detection systems [1–7]. In this method, a single trans-receiving antenna or a couple of antennas is used to scan the breast mechanically and synthetically generate the antenna array. On the other hand, recent work [8–10] has demonstrated that multistatic systems with a real aperture array offer a notable improvement for the imaging technique. Although several antennas have been suggested [11, 12] for use with CMI breast tumor detection, most of these antennas are either large or nonplanar and thus difficult for use as a base for an antenna array of several elements.

In a previous work, we have suggested an ultra-wideband (UWB) compact planar antenna design [13] that is easily fabricated using the

standard printed circuit board (PCB) process with embedded resistive technology. In this work, a new antenna design with a very wide-band behavior and an ultra-compact size is presented. This new design is simpler than the "Dark Eyes" antenna with an order of magnitude of improved performance. The antenna can be manufactured on Rogers Duroid 6010 high-frequency substrates [14] laminated with resistive conductive material (RCM) available from Ohmega Technologies [15]. In addition, the key advantage of this antenna is its strong forward-region radiation pattern. This makes the antenna a perfect candidate for a cross-polarized card-array arrangement as suggested in [16]. This new design will be a key element in developing the radar-based multistatic polarimetric breast cancer detection system.

2. ANTENNA DESIGN

The new proposed design named the Traveling Wave Tapered and Loaded Antenna (TWTLA) has evolved from the coplanar strip-fed miniaturized "Dark Eyes" antenna through several design modifications with the main objective to improve the antenna lower operating frequency and to further miniaturize it at the same time.

According to the *IEEE Standard Definitions of Terms for Antennas* [17], the antenna is a mean to radiate or receive radio waves. In other words, it is a transitional structure between free-space and a guiding device [18]. It could also be interpreted as a mode transformer that transforms a guided wave in a transmission line or a waveguide structure into a plane wave propagating in free-space [19]. This usually happens under matched condition and it is a key idea in developing traveling wave antennas. Furthermore, for broadband antennas, this matched condition should be satisfied within a broad range of frequencies. In addition, the above definition equally applies for radiating waves in a different background medium than free-space.

For a matched condition to happen, reflections should be minimized at the joint location of the transmission line guiding the wave and the antenna. In addition, the antenna itself should have a traveling wave nature. This led to the idea of merging the "Dark Eyes" antenna with its coplanar-strip feed to form one smooth tapered and resistively loaded structure that will guide the wave and radiate it into the background medium.

The evolution steps that transformed the "Dark Eyes" antenna into the TWTLA antenna are summarized next, but first we will present the initial development idea.

The antenna was simulated with SEMCAD [20], three-dimensional finite-difference (FDTD) solver, and with high-frequency structure

simulator (HFSS) [21]. In all simulations, the antenna was assumed to be printed on a dielectric board of dielectric constant $\epsilon_r = 10.2$ and immersed in a background medium of the same dielectric constant $\epsilon_r = 10.2$. The conductive and resistive layers were assumed to be 70-µm thick, and the resistive material has a surface resistivity $R_s = 50\,\Omega/\square$.

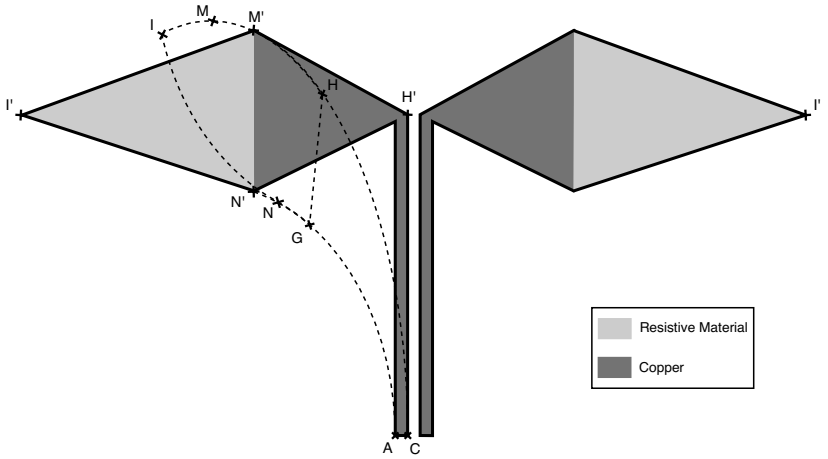

Figure 1. The original "Dark Eyes" antenna design with its CPS transmission line feed and the left arm of the evolved TWTLA final antenna design showing parameterization curves and points. Total width of the original "Dark Eyes" antenna, I'-to-I' (left point of the left arm to right point of the right arm), is 20 mm.

Figure 1 show the original miniaturized "Dark Eyes" antenna with its Coplanar Stripline (CPS) line feed and Fig. 2 present the return loss S_{11} computed with SEMCAD in the range 1–35 GHz. Although the antenna has a broad operating bandwidth, the return loss degrades below 3.12 GHz. With the objective of further miniaturizing the antenna and improve its lower operating frequency, one can employ the CPS line length to radiate the wave in a similar manner to the operating mechanism of tapered slot antennas (TSAs). This idea of combining a tapered transmission line with a resistively loaded section proves to be novel and does not suffer from the size limitation of typical traveling wave TSAs (length $L \geq 2\lambda$ and width $W \geq \lambda/2$) [19]. For example, the final TWTLA antenna can achieve a traveling behavior with a width much smaller than $\lambda/2$. Fig. 3 presents the initial idea developed using elliptical curves.

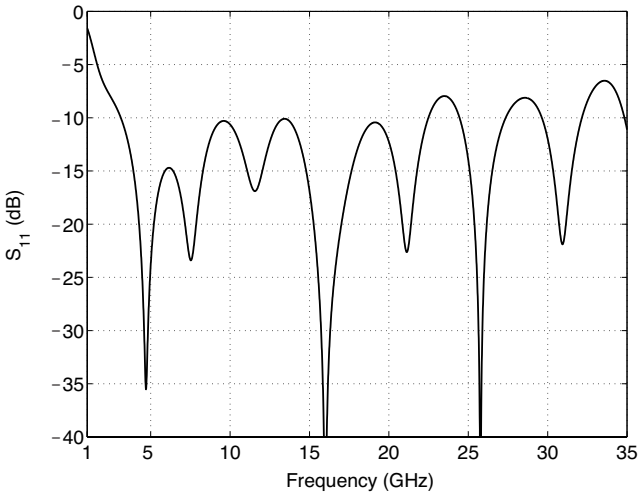

Figure 2. Return loss S_{11} of the original "Dark Eyes" antenna in the 1–35 GHz range, computed for a reference feedline with $R_{ref} = 50\,\Omega$. The antenna is immersed in a dielectric medium of $\epsilon_r = 10.2$. The return loss is below -10 dB in the 3.12–22.48 GHz range.

2.1. Characteristic Impedance of CPS and APS Lines

Since the TWTLA antenna is formed by tapering a transmission line, either a CPS line or an APS line, the design process starts by developing a transmission line with a desired characteristic impedance Z_0. In this section, we assume that the desired characteristic impedance is $Z_0 = 50\,\Omega$. However, the design process of a TWTLA antenna that is matched to any given reasonable Z_0 is identical.

Figure 4 shows a CPS structure. The characteristic impedance Z_0 of such a structure depends on the following parameters: the relative permittivity of the dielectric substrate ϵ_{rs}, the relative permittivity of the background material ϵ_{rb}, dielectric substrate height h, conducting strip width w, conducting strip thickness t, and the conducting strip separation s.

Two CPS line were designed on a substrate with $\epsilon_{rs} = 10.2$ and assumed to be immersed in the same background medium with $\epsilon_{rb} = 10.2$. The first one has the following dimensions: $w = 375\,\mu$m, $s = 375\,\mu$m, $t = 70\,\mu$m, and $h = 0.635$ mm. Using a two dimensional finite difference code, the characteristic impedance was computed to be $Z_0 = 61.8\,\Omega$. The characteristic impedance versus frequency was also computed using SEMCAD and HFSS in the 1–20 GHz range and it is

shown in Fig. 5. HFSS result, $Z_0(1\,\mathrm{GHz}) = 62\,\Omega$, is in close agreement with the finite difference code, while SEMCAD predicted a slightly lower value of $Z_0(1\,\mathrm{GHz}) = 52\,\Omega$.

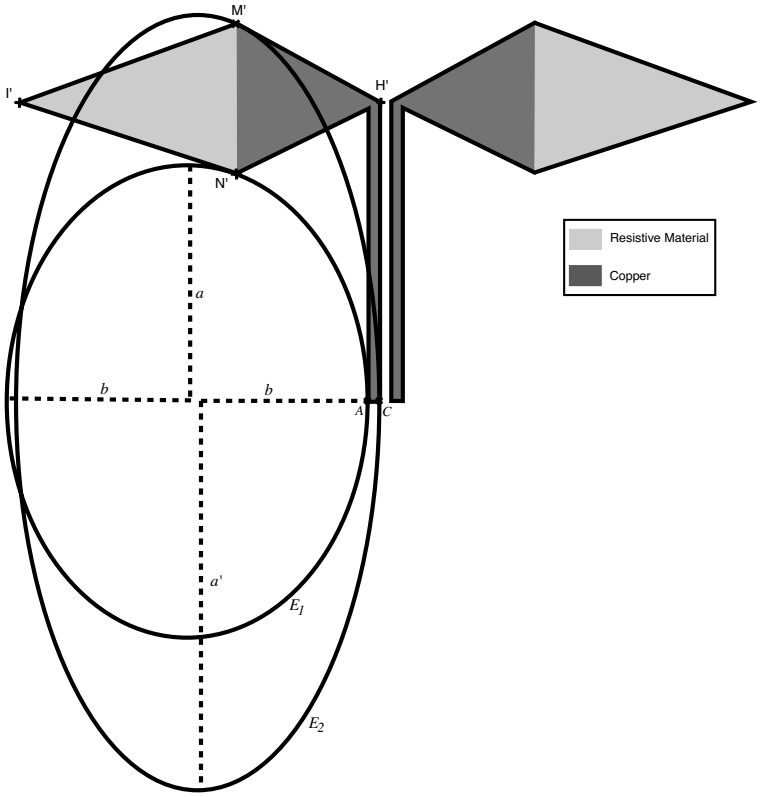

Figure 3. Illustration of the initial proposal to combine the CPS line feed and the initial metallic section of the original "Dark Eyes" antenna to form a single tapered transmission line section. Two ellipses E_1 with semimajor axis a and semiminor axis b, and E_2 with semimajor axis a' and semiminor axis b are used to form the tapered transmission line section. E_1 passes through point A and N' and it is tangent to line section N'I'. E_2 is a shifted version of E_1 that passes through point C and scaled along its major axis to pass through point M'.

A second CPS was designed which has the same dimensions as the first one except for the separation $s = 200\,\mu\mathrm{m}$. The characteristic impedance computed using the two dimensional finite difference code was found to be $Z_0 = 49.3\,\Omega$. Simulation results using SEMCAD and HFSS are presented in Fig. 6. Again, HFSS result, $Z_0(1\,\mathrm{GHz}) = 51\,\Omega$,

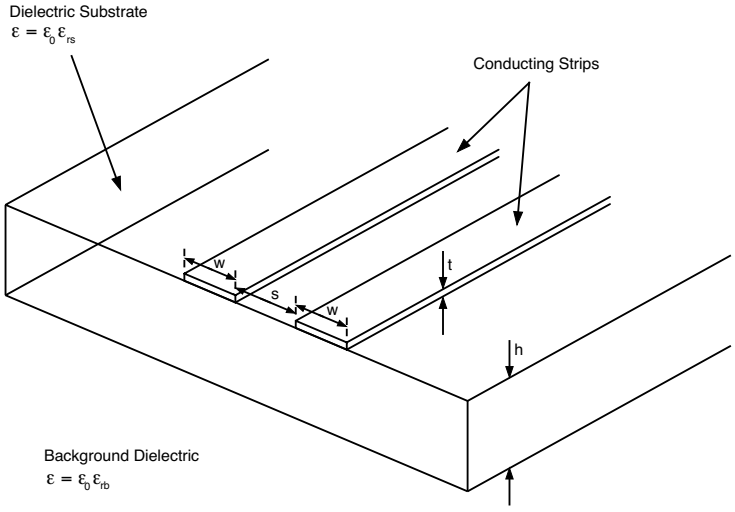

Figure 4. Coplanar stripline (CPS) configuration.

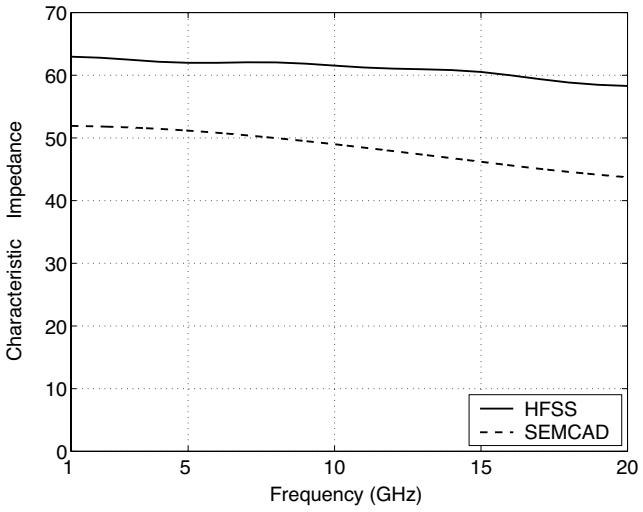

Figure 5. Characteristic impedance versus frequency for a CPS line printed on a dielectric board with a dielectric constant of $\epsilon_{rs} = 10.2$ and immersed in a background medium of dielectric constant $\epsilon_{rb} = 10.2$. The CPS dimensions are: $w = 375\,\mu\text{m}$, $s = 375\,\mu\text{m}$, and $t = 70\,\mu\text{m}$. The board thickness is $h = 0.635\,\text{mm}$.

is in close agreement with the finite difference code, while SEMCAD predicted a slightly lower value of $Z_0(1\,\mathrm{GHz}) = 43\,\Omega$.

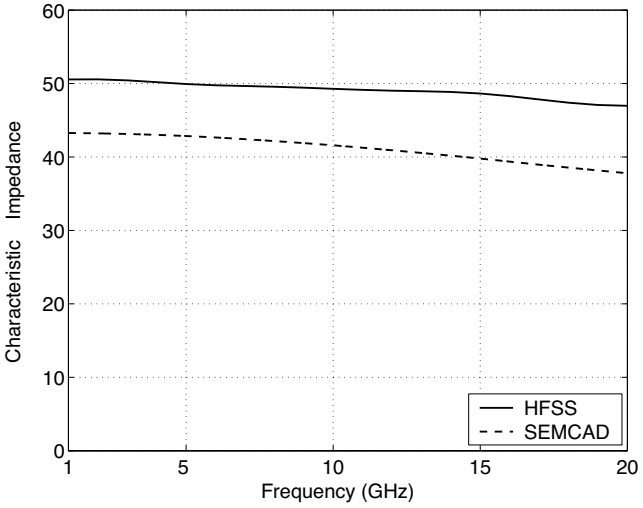

Figure 6. Characteristic impedance versus frequency for a CPS line printed on a dielectric board with a dielectric constant of $\epsilon_{rs} = 10.2$ and immersed in a background medium of dielectric constant $\epsilon_{rb} = 10.2$. The CPS dimensions are: $w = 375\,\mu\mathrm{m}$, $s = 200\,\mu\mathrm{m}$, and $t = 70\,\mu\mathrm{m}$. The board thickness is $h = 0.635\,\mathrm{mm}$.

An important step in the design of a broadband antenna is the choice of a suitable feeding technique. In order to open the possibility of using a direct microstrip feed in a similar manner to the microstrip fed antipodal Vivaldi antenna [22], APS line was also designed and used to develop the TWTLA antenna.

Figures 7–9 show the three possible configurations of an APS line. Depending on the background medium (ϵ_{rb}) and the substrate characteristics (ϵ_{rs}, h and t), one configuration might be more suitable than the others to achieve a given characteristic impedance Z_0.

With the objective of designing an APS line with a characteristic impedance as close to $50\,\Omega$ as possible and with similar dimensions to the CPS line presented above, an APS line with overlapping strip edges with the following dimensions was designed: $w = 375\,\mu\mathrm{m}$, $s = 100\,\mu\mathrm{m}$, $t = 70\,\mu\mathrm{m}$, and $h = 0.635\,\mathrm{mm}$. The dielectric constant of the background medium and the board was considered to be 10.2.

Using the two-dimensional finite-difference code, the characteristic impedance was computed to be $Z_0 = 65.2\,\Omega$. Simulation results using HFSS and SEMCAD are also plotted in Fig. 10. HFSS result,

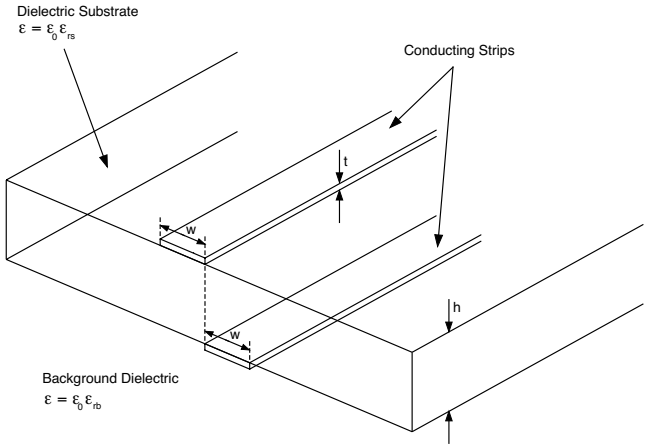

Figure 7. Antipodal stripline (APS) configuration with even strip edges.

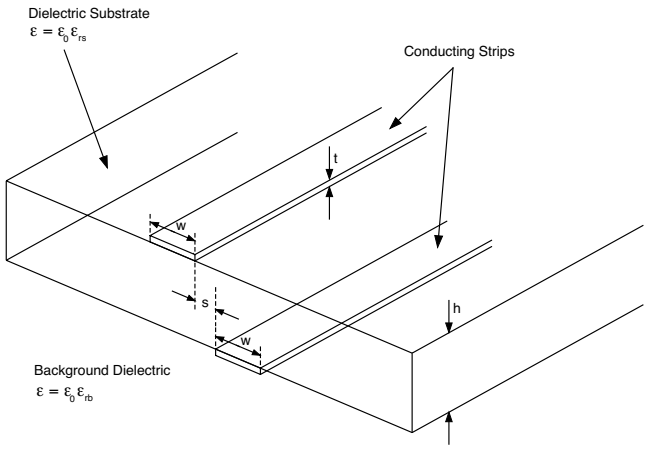

Figure 8. Antipodal stripline (APS) configuration with separated strip edges.

$Z_0(1\,\mathrm{GHz}) = 67\,\Omega$, are again in close agreement with the finite difference code, while SEMCAD predicted a slightly lower value of $Z_0(1\,\mathrm{GHz}) = 62\,\Omega$ and further decreases a higher frequency.

As we can see, the characteristic impedance of the APS line is slightly higher than the desired value of $50\,\Omega$, however, simulation results in the following section will show that this will have a minor effect on the input return loss of the antipodal TWTLA antenna design.

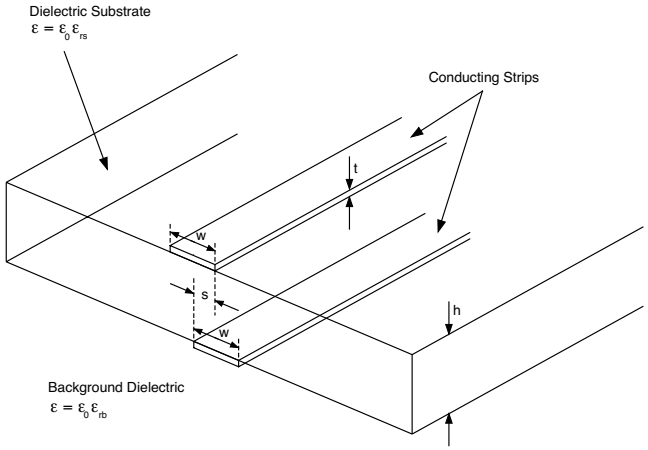

Figure 9. Antipodal stripline (APS) configuration with overlaping strip edges.

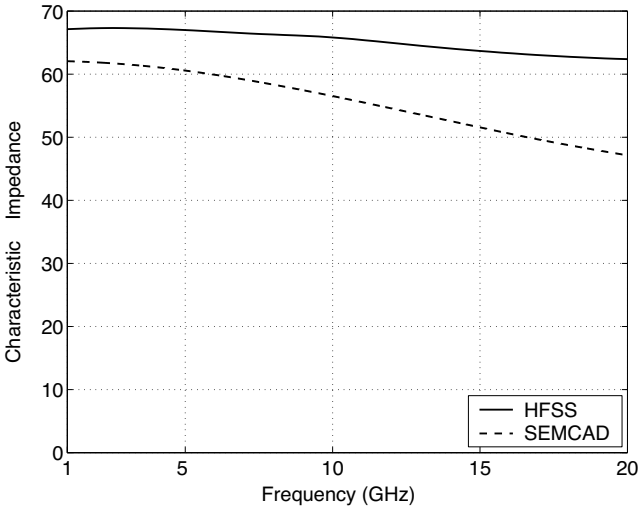

Figure 10. Characteristic impedance versus frequency for an APS line with overlaping strip edges. The APS line is printed on a dielectric board with a dielectric constant of $\epsilon_{rs} = 10.2$ and immersed in a background medium of dielectric constant $\epsilon_{rb} = 10.2$. The APS dimensions are: $w = 375\,\mu\text{m}$, $s = 100\,\mu\text{m}$, and $t = 70\,\mu\text{m}$. The board thickness is $h = 0.635\,\text{mm}$.

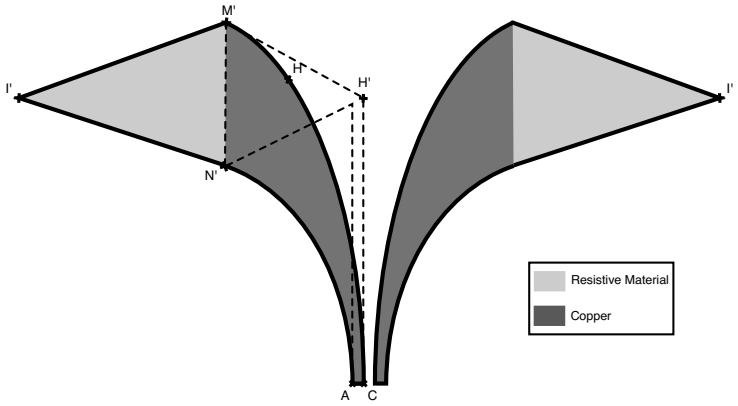

Figure 11. First stage in design evolution. Resistive area is the same as the one used in the "Dark Eyes" antenna and the total antenna width I'-to-I' is still 20 mm. In this design, the CPS feedline and the initial metallic section of the "Dark Eyes" antenna are merged to form a tapered elliptical transmission line defined by the ellipses shown in Fig. 3. This shows an improved return loss at higher frequencies, but a relatively degraded performance in the lower frequency range. This may be caused by the discontinuity that exists at point M' where both the material and the geometric form change.

2.2. Evolution Steps

Figures 11–17 depict the sequence of modifications and rationale that resulted in transforming the "Dark Eyes" antenna into the TWTLA antenna with a large improved performance. Unless otherwise stated, the return loss S_{11} of each evolved design is computed using SEMCAD and plotted for a reference impedance $R_{ref} = 50\,\Omega$.

Figure 11 presents the first evolved design. It is formed from the ellipses defined in Fig. 3. This design has an improved higher frequency performance, however, its lower frequency limit is rather high ($f_L = 4.43\,\text{GHz}$).

To improve the lower frequency operation of the antenna, the resistive area was increased by pushing back the border line between the different material toward the transmission line origin. In addition, this will eliminate the geometric discontinuity at the border line of the material. This process results in the second evolved design shown in Fig. 13. The antenna has a very large bandwidth with a lower frequency limit $f_L = 1.78\,\text{GHz}$. However, the increased size of the resistive area will further reduce the antenna efficiency.

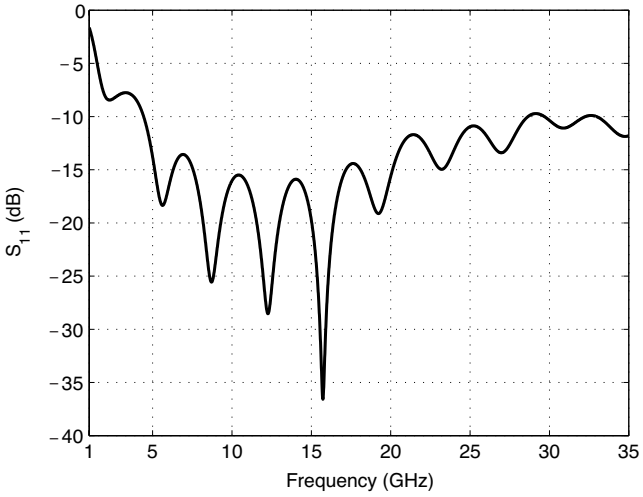

Figure 12. Return loss S_{11} of the first evolved design in the 1–35 GHz range, computed for a reference feedline with $R_{ref} = 50\,\Omega$. The antenna is immersed in a dielectric medium of $\epsilon_r = 10.2$. This design has a return loss below -10 dB in the 4.43–28.65 GHz range.

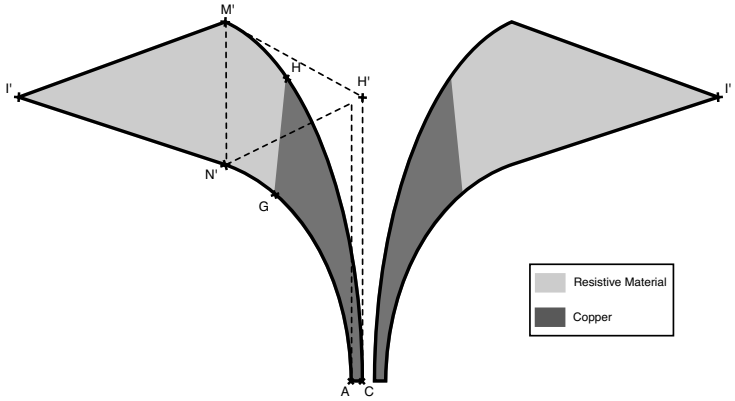

Figure 13. Second stage in design evolution. Here, the line M'N' (interface between different materials) is pushed back toward the transmission line origin and form the HG line. The behavior of this antenna improves significantly, however, the resistive area is now relatively large which implies lower antenna efficiency. The antenna width, I'-to-I', remains to be 20 mm.

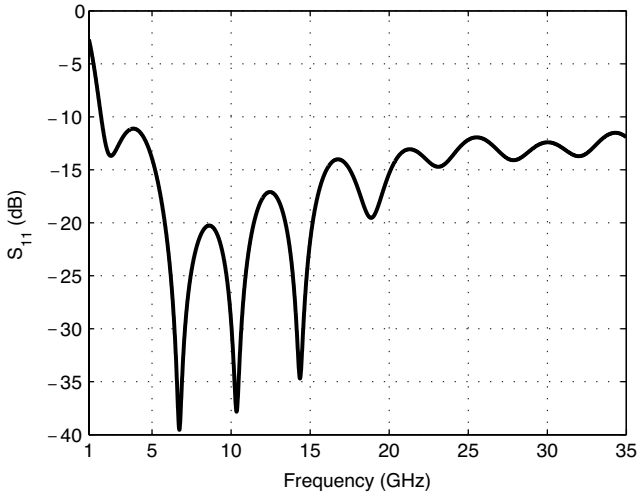

Figure 14. Return loss S_{11} of the second evolved design in the 1–35 GHz range, computed for a reference feedline with $R_{ref} = 50\,\Omega$. The antenna is immersed in a dielectric medium of $\epsilon_r = 10.2$. This design has a return loss below −10 dB in the 1.78–35 GHz range.

Figure 15 presents the third stage of the design evolution. Here, the objective was to reduce the size of the resistive area and the total antenna length while keeping the improved performance of the second evolved design. This was achieved through the geometrical modification explained step-by-step in the figure caption. This design has a total width of 16 mm and a lower frequency limit of $f_L = 1.84$ GHz.

Figure 17 presents the final design. In this design, all discontinuities are removed and the geometric taper of both antenna sections (conductive and resistive) is formed from smooth curves only (from the origin of the transmission line to the antenna ends). The figure caption explains in further detail how to construct the antenna taper. In this design, the total antenna width is further reduced to only 14 mm. For this design, the antenna return loss S_{11} was computed using both SEMCAD and HFSS for comparison and verification. The results computed with SEMCAD show a return loss below −10 dB in the 1.94–35 GHz range. For HFSS, the computed results show a return loss below −10 dB in the 1.73–34.37 GHz range. Simulation results for both SEMCAD and HFSS are in close agreement as can be seen in Fig. 18.

The above discussion summarized the steps that have led to the

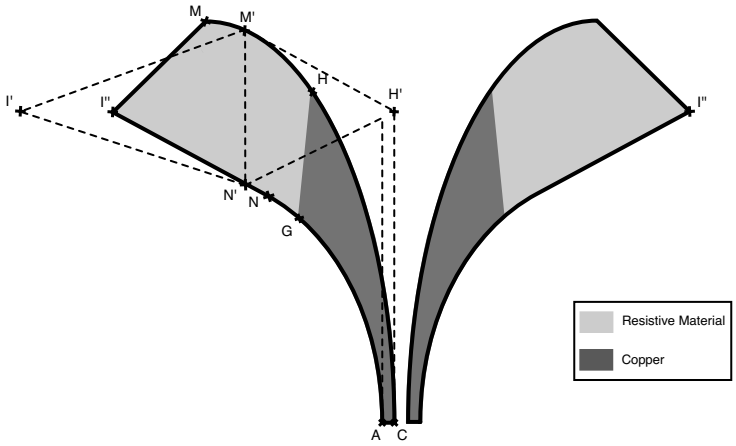

Figure 15. Third stage in design evolution. Here, an attempt to reduce the effect of the discontinuity at point M' is executed by pushing it further away on the CI curve up to point M and making the lossy path that the current has to travel longer before it intercepts the discontinuity. Then, the total antenna width is reduced by first pushing point N' slightly back to point N, and second by extending the line at point N in a tangent direction to intercept the line MI' at point I". In this manner, the lossy resistive area is reduced. The total antenna width, I"-to-I", is reduced to 16 mm.

development of the TWTLA. In addition, and through numerous numerical analysis, a design methodology and guideline for developing antipodal and coplanar TWTLA will be presented in the following section. However, an important point that needs to be stressed here is the fact that the antenna input impedance acquires the characteristic impedance of the original transmission line. Fig. 19 presents HFSS simulation results for the final antenna design of Fig. 17 referenced to both 50 Ω and 60 Ω. As we can see, since HFSS predicts a characteristic impedance of 60 Ω for the CPS line with separation $s = 375\,\mu m$ (as shown in Fig. 5), the antenna return loss improves when referenced to $R_{ref} = 60\,\Omega$. Fig. 19 also presents the HFSS simulation results for the final antenna design when developed from an identical CPS line but with a separation $s = 200\,\mu m$. Again, since HFSS predicts a characteristic impedance of 50 Ω for the CPS line with separation $s = 200\,\mu m$ (as shown in Fig. 6), this antenna is well matched to $R_{ref} = 50\,\Omega$.

Finally, Fig. 20 shows the results for the TWTLA developed from the APS line of Fig. 10. When referenced to 50 Ω, the results computed

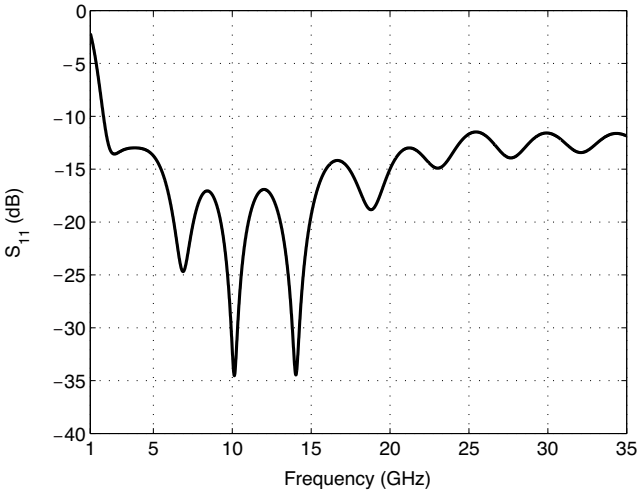

Figure 16. Return loss S_{11} of the third evolved design in the 1–35 GHz range, computed for a reference feedline with $R_{ref} = 50\,\Omega$. The antenna is immersed in a dielectric medium of $\epsilon_r = 10.2$. This design has a return loss below −10 dB in the 1.84–35 GHz range.

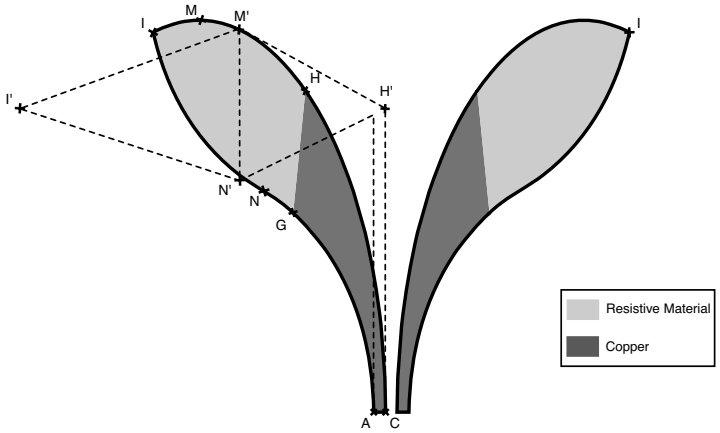

Figure 17. The final design. First, the discontinuity at point M is removed by extending the elliptic curve to point I where it is intercepted by another elliptical curve NI. In this manner, all discontinuities are removed and the antenna total width, I-to-I, is further reduced to only 14 mm.

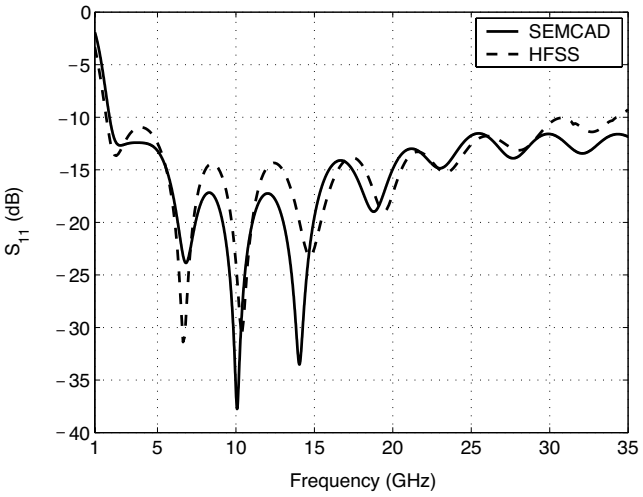

Figure 18. Return loss S_{11} of the final antenna design in the 1–35 GHz range, computed for a reference feedline with $R_{ref} = 50\,\Omega$. The antenna is immersed in a dielectric medium of $\epsilon_r = 10.2$. The results computed with SEMCAD show a return loss below -10 dB in the 1.94–35 GHz range. For HFSS, the computed results show a return loss below -10 dB in the 1.73–34.37 GHz range.

with SEMCAD show that the minimum lower operating frequency of -10 dB return loss is 2.14 GHz while, for results computed with HFSS, it is 1.97 GHz. As we can see, the antipodal design has similar performance to the coplanar version. Again, simulation results have shown that the antenna input impedance is well matched to $60\,\Omega$ and not $50\,\Omega$. This is explained by the fact that the APS used to develop the antenna has a characteristic impedance slightly higher than $50\,\Omega$ (as shown in Fig. 10).

2.3. Design Rules: Guidelines for the TWTLA Antenna

1- Depending whether it is desired for the antenna to be coplanar or antipodal, begin by designing a CPS or an APS transmission line with the desired characteristic impedance Z_0 (the final antenna design will have an input impedance matched to Z_0).

Note: Antipodal antennas have usually higher cross-polarization radiation than their planar counterpart, however it is easier to design a broadband matching feed for the antipodal structure.

2- Once the CPS or the APS is designed (in a specific background

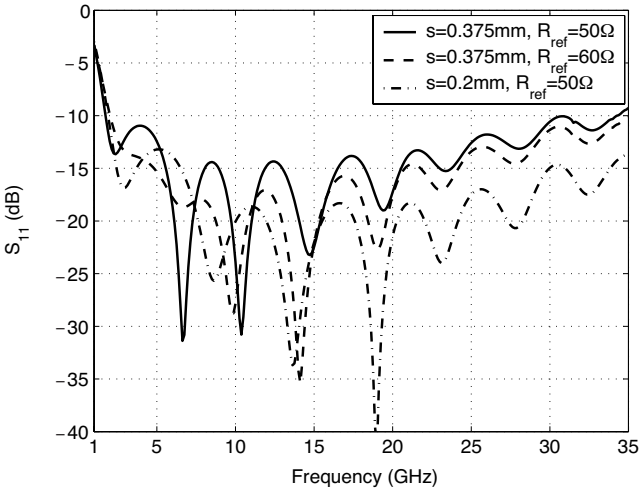

Figure 19. Return loss S_{11} of the final antenna design in the 1–35 GHz range computed with HFSS. The solid line curve is for the antenna with a separation $s = 375\,\mu\text{m}$ and referenced to a $50\,\Omega$ feedline while the dashed line curve is for the same antenna when referenced to a $60\,\Omega$ feedline. The dash-dot line curve is for the antenna with a separation $s = 200\,\mu\text{m}$ and referenced to a $50\,\Omega$ feedline. The antenna is immersed in a dielectric medium of $\epsilon_r = 10.2$.

medium that the antenna is supposed to radiate in), taper every conducting strip of the CPS or the APS following the geometric dimensions given in Fig. 21. This will lead to an almost optimal TWTLA antenna design.

a. Path "AC" corresponds to the conducting strip width w.

b. The resistive material should have a surface resistivity R_s. A good choice for R_s is $50\Omega/\square$, however, the optimal R_s value for a specific medium should be determined through simulations and experiments.

c. λ is the wavelength in the radiating medium corresponding to the lower operating frequency f_L of the antenna.

d. Path "CHMI" is elliptical, but it could also be exponential, or any function of a similar form. However, it is advisable to keep all curves smooth, i.e., to have a continuous second-order derivative at any joining point. The same holds for path "AGN" and path "NI".

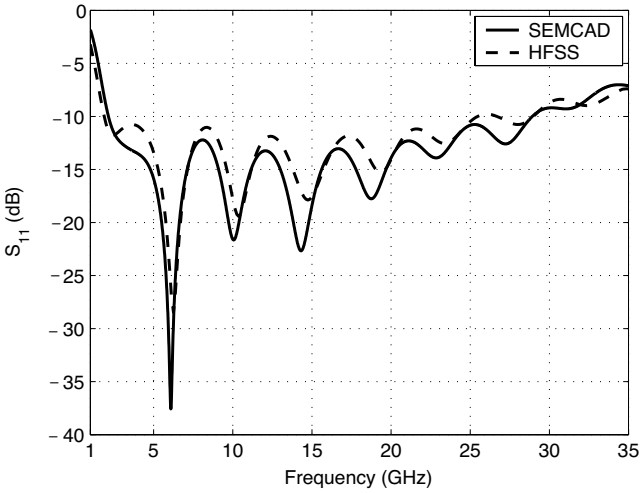

Figure 20. Return loss S_{11} of the final antenna design when developed from an antipodal stripline APS with overlaping strip edges of $s = 100\,\mu$m. The results are shown in the 1–35 GHz range and referenced to a 50 Ω feedline. The results computed with SEMCAD show that the minimum lower operating frequency of −10 dB return loss is 2.14 GHz, while for results computed with HFSS it is 1.87 GHz.

e. Points H and G are used to further optimize the antenna. They are also dependent on the available surface resistivity R_s.

f. Conducting strip separation s at the origin of the antenna design should be the same as in the CPS or the APS design. In fact, a transverse plane cut at the origin of the antenna should be identical to any transverse plane cut in the CPS or the APS design.

3. ANTENNA CHARACTERISTICS IN THE UWB RANGE

Since the antenna is intended for use in confocal microwave imaging of breast cancer and similar near-field sensing applications, it is important to characterize its pulse radiation performance in the UWB range and in the near-field.

The antenna was simulated with SEMCAD as it is easier to analyze the pulse response in time domain. The excitation pulse is shown in Fig. 22. It consists of a Gaussian-modulated sinusoidal

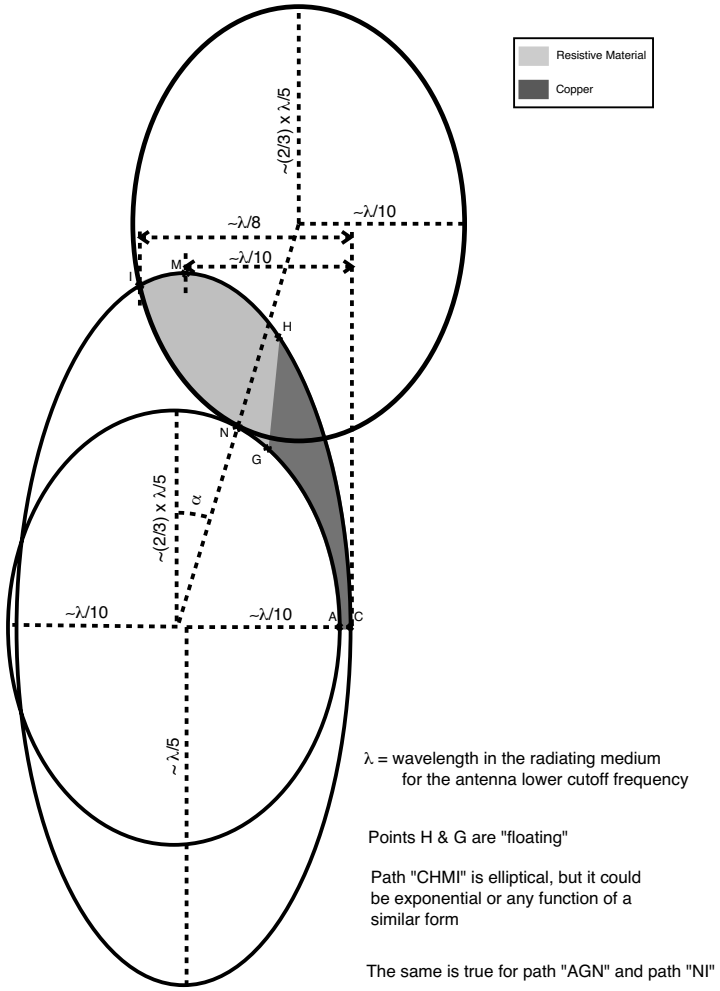

Figure 21. Detailed antenna geometry and electrical dimensions associated with a matching medium of dielectric constant ϵ_r and designed for a specific minimum lower operating frequency $f_L = c/(\lambda\sqrt{\epsilon_r})$.

waveform mathematically described by:

$$\mathcal{V}(t) = \sin[2\pi f_0(t - t_0)] \exp\left[-(t - t_0)^2/2\tau^2\right] \tag{1}$$

with $f_0 = 6\,\text{GHz}$, $\tau = 80\,\text{ps}$, and $t_0 = 5\tau$. This pulse has a temporal width of 0.19 ns (full width at half maximum-FWHM). Its is centered at 6 GHz with a spectral width of 4.4 GHz (FWHM) and no dc content.

Simulation results for the antenna efficiency, near-field radiation and fidelity are presented next.

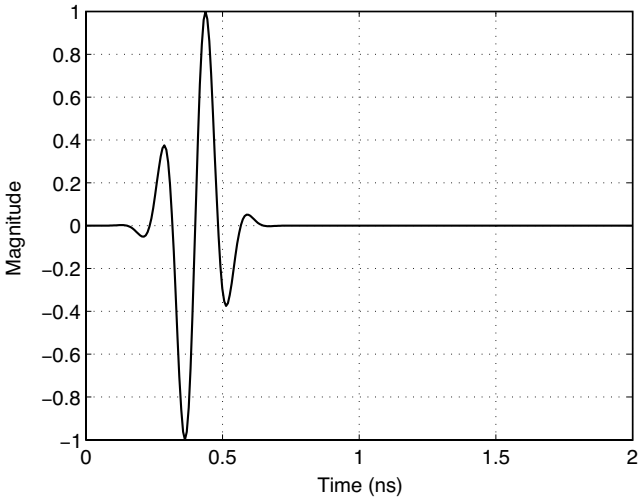

Figure 22. Waveform of the Gaussian modulated sine described by Eqn. 1.

3.1. Efficiency

Table 1 presents the calculated antenna efficiency and the percentage distribution of the total energy of the pulse incident from the feedline. As we can see, the antenna efficiency is relatively high when compared to typical resistively loaded antennas [23]. However, it important to note these results are dependent on the excitation waveform and its spectral content.

Table 1. Percentage distribution of the total incident energy from a feedline with $R_{ref} = 50\,\Omega$.

Antenna Surface Resistivity	Reflected Energy	Dissipated Energy	Radiated Energy	Radiation Efficiency
$R_s = 50\,\Omega/\square$	2.82%	59.08%	38.1%	39.21%

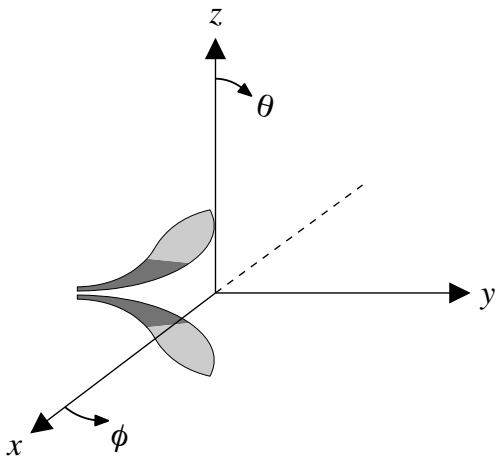

Figure 23. Antenna orientation in polar coordinates.

3.2. Near-field Radiation and Antenna Fidelity

The antenna pulse performance in the UWB range can be characterized by fidelity (F) of the radiated field in time domain. It is a measure of distortion in the radiated waveform as it propagates away from the antenna and it is defined as the maximum cross-correlation between the time derivative of the exciting pulse $\mathcal{V}(t)$ and the radiated electric field $\mathcal{E}_\theta^r(t)$ as such [24]:

$$F = \max_\tau \int_{-\infty}^{+\infty} \tilde{r}(t)\tilde{\mathcal{E}}_\theta^r(t+\tau)dt, \tag{2}$$

where $\tilde{r}(t) = d\tilde{\mathcal{V}}(t)/dt$ and $\tilde{\mathcal{E}}_\theta^r(t)$ are normalized to their respective energies. With this definition, the fidelity ranges from 0 to 1 with $F = 1$ indicating a perfect match between $\tilde{r}(t)$ and $\tilde{\mathcal{E}}_\theta^r(t)$.

Since we are interested in sensing applications in the near-field, the antenna fidelity was computed at 3 cm radial distance from the antenna apex in the E- and H-plane. Figs. 24 and 25 present the transient radiated electric field waveform $\tilde{\mathcal{E}}_\theta^r(t)$ in a 180° span in the forward region. By visual inspection, it is possible to observe that the radiated waveform is approximately the time derivative of the exciting signal given by Eqn. 1. For a quantitative measure, Table 2 presents the computed fidelity at several observation angle in the E- and H-plane. As we can see, except for fidelity at 90° angles off boresight in

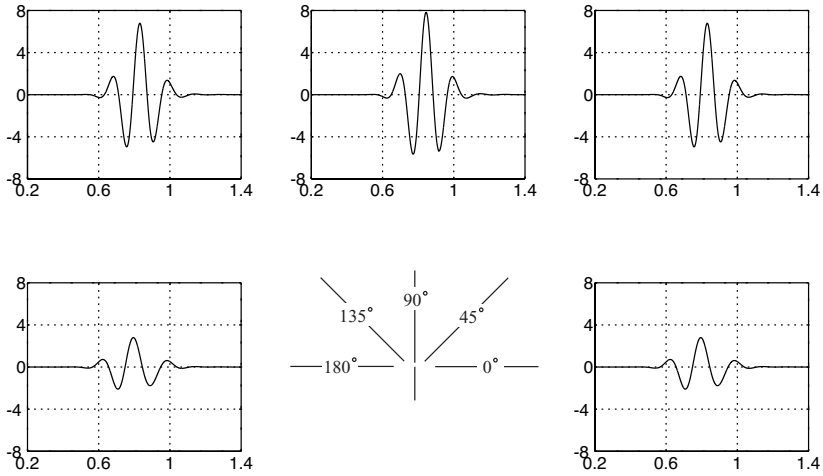

Figure 24. Radiated electric field waveform computed at 3 cm radial distance from the antenna apex in the H-plane and as a function of the polar angle ϕ.

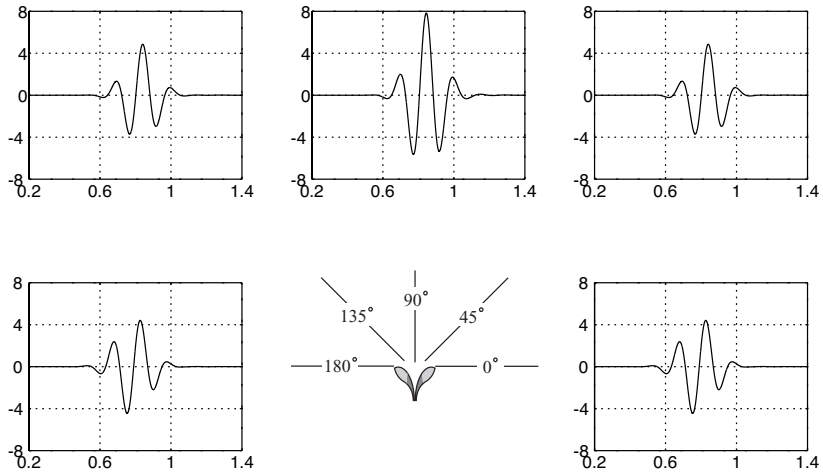

Figure 25. Radiated electric field waveform computed at 3 cm radial distance from the antenna apex in the E-plane and as a function of the polar angle θ.

the H-plane ($\theta = 90$ plane), the antenna fidelity is excellent and it is over 0.95.

Finally, the antenna near-field radiation patterns computed at

Table 2. Radiated electric field fidelity F at selected polar angles.

Polar angles: θ or ϕ / Radiation Plane	$0°$	$22.5°$	$45°$	$67.5°$	$90°$
H-plane ($\theta = 90°$)	0.821	0.958	0.989	0.996	0.997
E-plane ($\phi = 90°$)	0.959	0.977	0.986	0.993	0.997

3 cm radial distance from the antenna apex are presented. Figs. 26 and 27 give the magnitude of the radiated electric field in the H-plane and E-plane at three selected frequencies across the UWB span: 3 GHz, 6 GHz, and 9 GHz. As we can see, the antenna near-field radiation is relatively uniform in the H-plane with a half-power beamwidth of 183.20°, 124.96°, and 99.68° at 3 GHz, 6 GHz, and 9 GHz respectively. In the E-plane, the near-filed radiated intensity varies slightly, however, the -3 dB beamwidth is still wide and equal to 101.81°, 78.30°, and 77.73° at 3 GHz, 6 GHz, and 9 GHz, respectively.

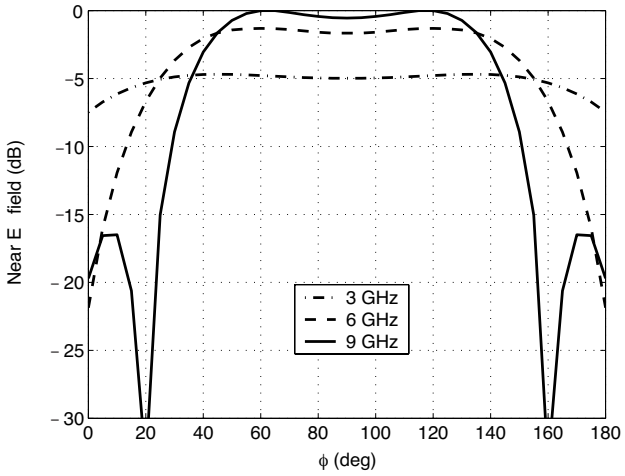

Figure 26. Antenna near E-field magnitude computed at 3 cm radial distance from the antenna apex in the H-plane at three selected frequencies: 3 GHz, 6 GHz, and 9 GHz.

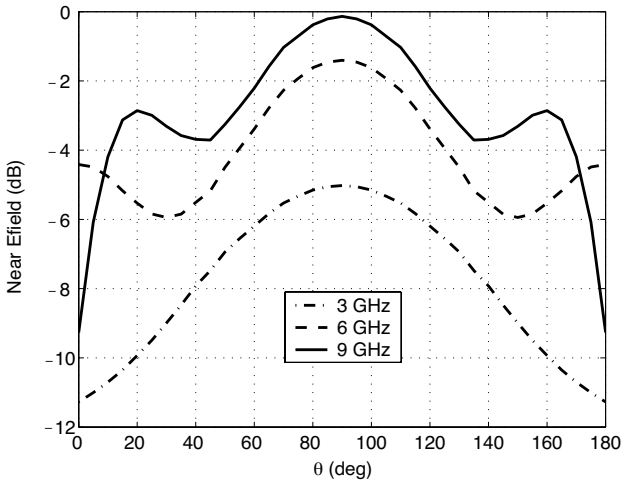

Figure 27. Antenna near E-field magnitude computed at 3cm radial distance from the antenna apex in the E-plane at three selected frequencies: 3 GHz, 6 GHz, and 9 GHz.

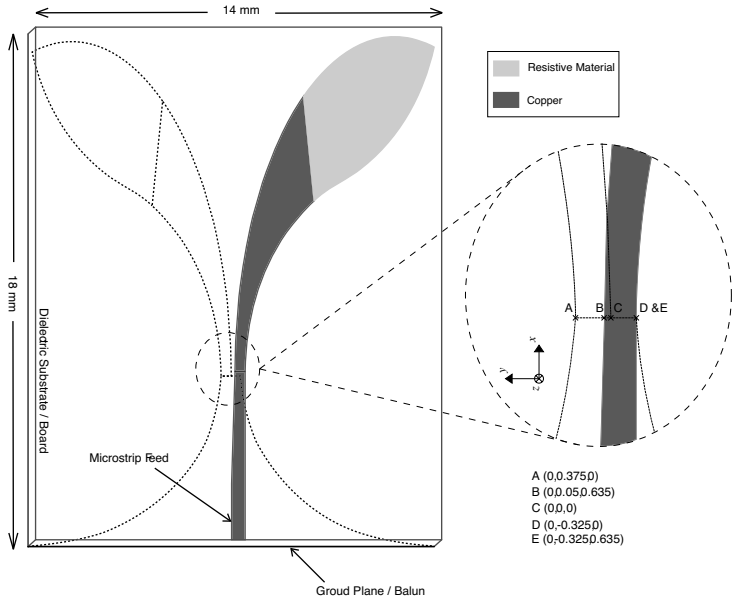

Figure 28. Antenna board view. Coordinate dimensions are in mm.

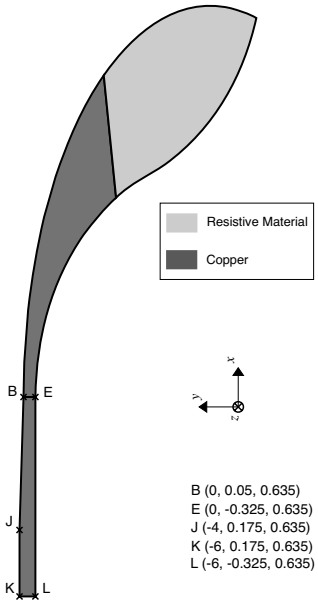

Figure 29. Antenna's top plane art work (top view). Coordinate dimensions are in mm.

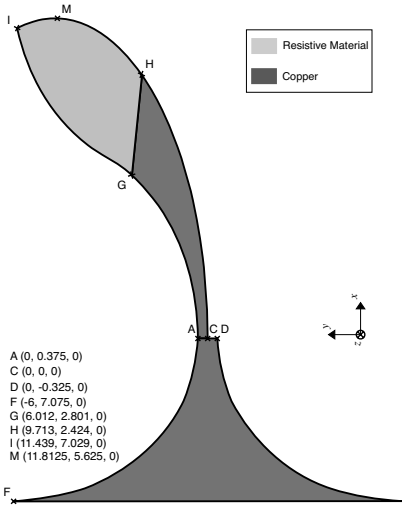

Figure 30. Antenna's bottom plane art work (top view). Coordinate dimensions are in mm.

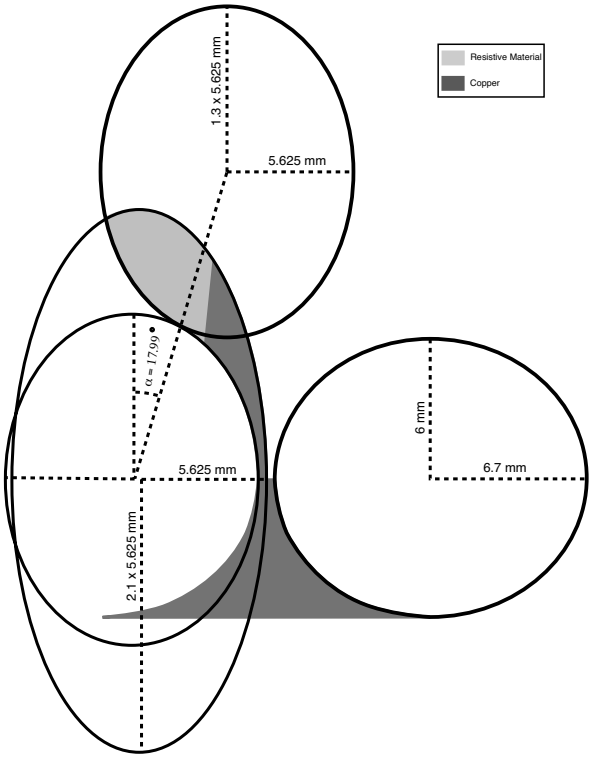

Figure 31. Detailed antenna geometry and absolute physical dimensions derived from elliptical shapes and including the tapered feed/balun.

4. BALUN DESIGN

Figure 28 shows the antenna design with the balun/feed as it will be manufactured on a printed circuit board. It consists of a top layer, a dielectric substrate, and a bottom layer.

The detailed dimensions of the top layer are shown in Fig. 29. First, we see a copper section consisting of a linearly tapered microstrip feed connected to the elliptical radiating element. Second, the elliptical tapered resistive section serves as a partially radiating partially dissipating element. Fig. 30 shows the detailed dimensions of the bottom layer. The first section consists of an elliptical tapered copper section forming the ground plane/balun. In fact, using a tapered ground plane as a balun is the approach that led to the development of the TWTLA in its both versions, coplanar and antipodal. In this

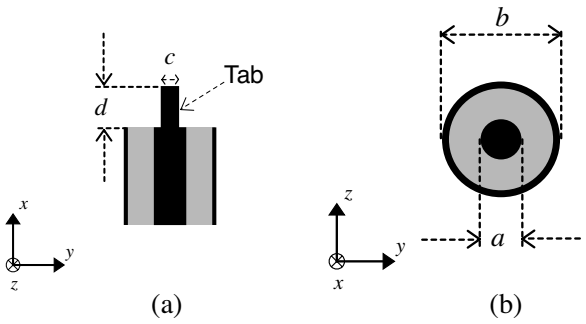

Figure 32. Geometry of the SMA connector used in the HFSS simulations: (a) Cross-section in the x-y plane, (b) Cross-section in the y-z plane. SMA dimensions (in mm): $a = 1.25$, $b = 4.2$, $c = 0.5$, and $d = 2$. The attached tab has a thickness of 0.5 mm. The SMA connector was assumed to be filled with Teflon with a dielectric constant $\epsilon_r = 2.1$.

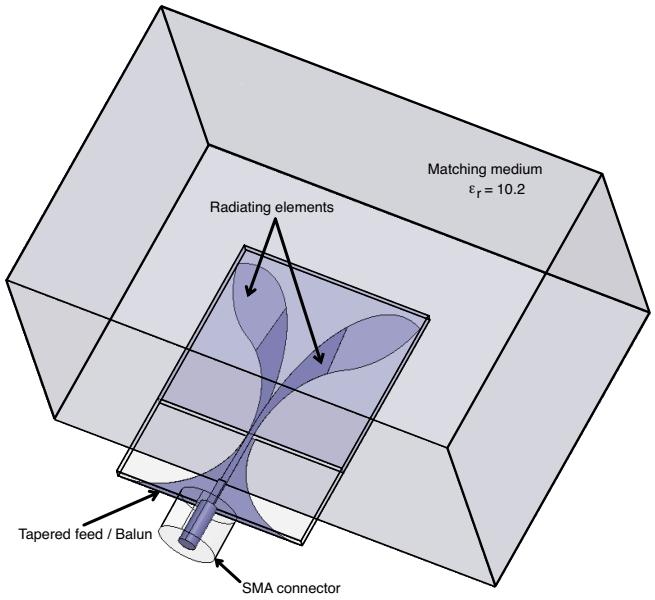

Figure 33. The radiating elements of the antenna are immersed in a matching medium of $\epsilon_r = 10.2$. The tapered feed/balun is kept in free space.

way, the balun design is not limited to only coplanar structures. The second and the third sections form the radiating/dissipating elements of this layer and they are identical to the one of the top layer. Finally, Fig. 31 presents the ellipses dimensions and orientation used to define both the radiating elements and the tapered balun.

To test the performance of the antenna design with the tapered ground-plane feed, it was simulated using both HFSS and SEMCAD. In addition, a subminiature version A (SMA) connector was designed to simulate the complete antenna structure. The SMA connector was simulated as a co-axial termination with a rectangular tab connected to its center conductor. The SMA is shown in Fig. 32. Its dimensions and characteristics are close to the commercially available hardware [25].

Figure 33 presents the simulation environment of the antenna. As it can be seen, the antenna is designed in such a way to be partially inserted as a card in a slot of some dielectric matching medium. The SMA connector and the microstrip/balun feed are supposed to be kept in free space. Only the radiating element of the antenna is immersed in the matching medium.

Figure 34 presents the return loss S_{11} of the final antenna design with the microstrip balun/feed but without the SMA connector. The results are shown in the 1–35 GHz range and referenced to a 50 Ω

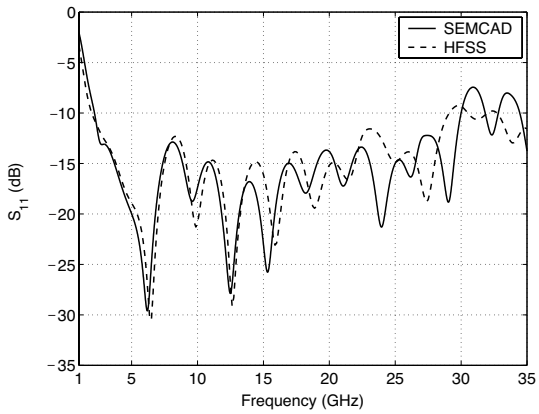

Figure 34. Return loss S_{11} of the final antenna design with the microstrip balun/feed simulated using both SEMCAD and HFSS but without the SMA connector. The results are shown in the 1–35 GHz range and referenced to a 50 Ω feedline. The results computed with SEMCAD show that the minimum lower operating frequency of −10 dB return loss is 2.18 GHz, while for results computed with HFSS it is 1.97 GHz.

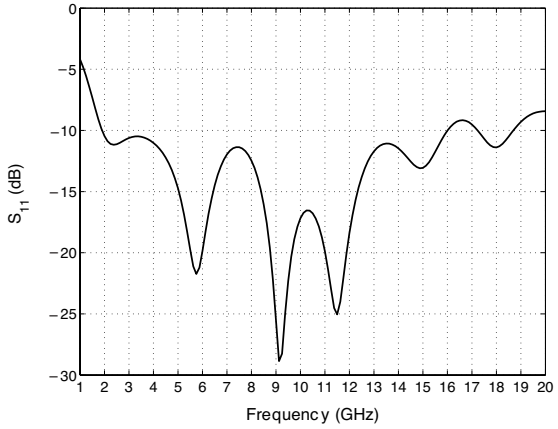

Figure 35. Return loss S_{11} of the final antenna design with the microstrip balun/feed and the SMA connector simulated with HFSS. The results are shown in the 1–20 GHz range and referenced to a 50 Ω feedline. As we can see from the plot, the antenna has a broad operating bandwidth of −10 dB return loss ranging from 1.9 GHz to 16.0 GHz. The high frequency operation becomes limited by the SMA to microstrip transition.

feedline. As we can see, the results are similar to those computed for the radiator only with a return loss below −10 dB starting from around 2 GHz to almost 30 GHz. When the SMA is present, the higher limit of the return loss of the antenna bandwidth is limited to 16 GHz. This is mainly due to the coax-to-microstrip transition.

5. CONCLUSION

In this paper, a novel ultra-compact and ultra-broadband antenna design, named the TWTLA antenna, is proposed for pulse radiation in the near-field. The antenna derives its name from its design procedure and its operation mechanism. The antenna has a return loss below −10 dB in the range of 1.9 GHz to 35.0 GHz. The antenna was also studied for pulse radiation in the UWB range. Its radiation efficiency is 39.21%. In the forward region, the computed fidelity at 3 cm radial distance from the antenna apex is over 0.95 within a span of 180° angles in the E-plane and a span of 135° angles in the H-plane. The antenna has a planar structure of only 18 mm × 14 mm. With this dimension, the antenna is the smallest of all reported designs up to date for the application of UWB microwave imaging of breast cancer. This antenna

will be a key element in developing a multistatic microwave imaging system with a large number of cross-polarized antenna-elements.

REFERENCES

1. Fear, E. C., P. M. Meaney, and M. A. Stuchly, "Microwaves for breast cancer detection?" *IEEE Potentials*, Vol. 22, 12–18, Feb. 2003.
2. Bond, E. J., X. Li, S. C. Hagness, and B. D. V. Veen, "Microwave imaging via space-time beamforming for early detection of breast cancer," *IEEE Trans. Antennas Propagat.*, Vol. 51, 1690–1705, Aug. 2003.
3. Guo, B., Y. Wang, J. Li, P. Stoica, and R. Wu, "Microwave imaging via adaptive beamforming methods for breast cancer detection," *Journal of Electromagnetic Waves and Applications*, Vol. 20, 53–63, 2006.
4. Zainud-Deen, S. H., W. M. Hassen, E. M. Ali, K. H. Awadalla, and H. A. Sharshar, "Breast cancer detection using a hybrid finite difference frequency domain and particle swarm optimization techniques," *Progress In Electromagnetics Research B*, Vol. 3, 35–46, 2008.
5. Bindu, G., A. Lonappan, V. Thomas, C. K. Aanandan, and K. T. Mathew, "Active microwave imaging for breast cancer detection," *Progress In Electromagnetics Research*, PIER 58, 149–169, 2006.
6. Bindu G., A. Lonappan, V. Thomas, C. K. Aanandan, and K. T. Mathew, "Dielectric studies of corn syrup for applications in microwave breast imaging," *Progress In Electromagnetics Research*, PIER 59, 175–186, 2006.
7. Zhang, H., S. Y. Tan, and H. S. Tan, "A novel method for microwave breast cancer detection," *Progress In Electromagnetics Research*, PIER 83, 413–434, 2008.
8. Nilavalan, R., A. Gbedemah, I. J. Craddock, X. Li, and S. C. Hagness, "Numerical investigation of breast tumour detection using," *Electronics Letters*, Vol. 39, 1787–1789, Dec. 2003.
9. Xie, Y., B. Guo, L. Xu, J. Li, and P. Stoica, "Multi-static adaptive microwave imaging for early breast cancer detection," *Proceedings of the 39th ASILOMAR Conference on Signals, Systems, and Computers*, Pacific Grove, Calif, USA, Oct. 2005.
10. Shao, W., B. Zhou, Z. Zheng, and G. Wang, "UWB microwave imaging for breast tumor detection in inhomogeneous tissue,"

Proceedings of IEEE Engineering in Medicine and Biology 27th Annual International Conference, 1496–1499, Shanghai, China, Sept. 2005.

11. Li, X., S. C. Hagness, M. K. Choi, and D. W. van der Weide, "Numerical and experimental investigation of an ultrawideband ridged pyramidal horn antenna with curved launching plane for pulse radiation," *IEEE Trans. Antennas Propagat.*, Vol. 2, 259–262, Feb. 2003.
12. Yun, X., E. C. Fear, and R. H. Johnston, "Compact antenna for radar-based breast cancer detection," *IEEE Trans. Antennas Propagat.*, Vol. 53, 2374–2380, Aug. 2005.
13. Kanj, H. and M. Popovic, "Miniaturized microstrip-fed 'Dark Eyes' antenna for near-field microwave sensing," *IEEE Antennas Wireless Propagat. Lett.*, Vol. 4, 397–401, 2005.
14. (2007) Rogers website. [Online]. Available: http://www.rogerscorporation.com
15. (2007) Ohmega website. [Online]. Available: http://www.ohmega.com/
16. Kanj, H. and M. Popovic, "T- and X-arrangement of 'Dark Eyes' antennas for microwave sensing array," *Proc. IEEE AP-S International Symposium*, 1111–1114, Albuquerque, NM, July 2006.
17. *IEEE Standard Definitions of Terms for Antennas*, IEEE Std. 145-1993, New York, 1993.
18. Balanis, C., *Antenna Theory*, John Wiley & Sons, Inc., New York, NY, 1997.
19. Lee, K. F. and W. Chen, *Advances in Microstrip and Printed Antennas*, John Wiley & Sons, Inc., New York, NY, 1997.
20. (2007) SEMCAD website. [Online]. Available: http://www.semcad.com/
21. (2007) Ansoft website. [Online]. Available: http://www.ansoft.com/
22. Gazit, E., "Improved design of the vivaldi antenna," *IEE Proc., Part H*, Vol. 135, No. 2, 89–92, 1988.
23. Montoya, T. P. and G. S. Smith, "A study of pulse radiation from several broad-band loaded monopoles," *IEEE Trans. Antennas Propagat.*, Vol. 44, 1172–1182, Aug. 1996.
24. Lamensdorf, D. and L. Susman, "Baseband-pulse-antenna techniques," *IEEE Antennas Propagat. Mag.*, Vol. 36, 20–30, Feb. 1994.
25. (2007) Johnson components. [Online]. Available: http://www.emersonnetworkpower.com